Report No. NAWCADWAR-95027-4.3

FIBER OPTIC BRAGG GRATING MODEL

Ignacio Perez and Thomas Bibby
Air Vehicle Department
Materials Division (Code 4.3.4.2)
NAVAL AIR WARFARE CENTER
AIRCRAFT DIVISION WARMINSTER
P.O. 5152
Warminster, PA 18974-0591

Marty Ryan
NAVMAR APPLIED RESEARCH CORPORATION
Warminster, PA 18974

1 JUNE 1995

FINAL REPORT

Approved for Public Release; Distribution is Unlimited.

Prepared for
Dr. Asha Varma
Group Head Engineering (Code 4.0C)
NAVAL AIR WARFARE CENTER
AIRCRAFT DIVISION WARMINSTER
P.O. Box 5152
Warminster, PA 18974-0591

NOTICES

REPORT NUMBERING SYSTEM - The numbering of technical project reports issued by the Naval Air Warfare Center, Aircraft Division, Warminster is arranged for specific identification purposes. Each number consists of the Center acronym, the calendar year in which the number was assigned, the sequence number of the report within the specific calendar year, and the official 2-digit correspondence code of the Functional Department responsible for the report. For example: Report No. NAWCADWAR-95010-4.6 indicates the tenth Center report for the year 1995 and prepared by the Crew Systems Engineering Department. The numerical codes are as follows.

Code	Department
4.1	Systems Engineering Department
4.2	Cost Analysis Department
4.3	Air Vehicle Department
4.4	Propulsion and Power Department
4.5	Avionics Department
4.6	Crew Systems Engineering Department
4.10	Conc. Analy., Eval. and Plan (CAEP) Department

PRODUCT ENDORSEMENT - The discussion or instructions concerning commercial products herein do not constitute an endorsement by the Government nor do they convey or imply the license or right to use such products.

Reviewed By: _____ Author/COTR Date: 7/5/95

Reviewed By: _____ ~~LEVEL III Manager~~ Date: 7/5/95

REPORT DOCUMENTATION PAGE

Form Approved
OMB No. 0704-0188

1. AGENCY USE ONLY *(Leave blank)*	2. REPORT DATE	3. REPORT TYPE AND DATES COVERED
	1 JUNE 1995	FINAL

4. TITLE AND SUBTITLE

FIBER OPTIC BRAGG GRATING MODEL

5. FUNDING NUMBERS

6. AUTHOR(S)

IGNACIO PEREZ and THOMAS BIBBY*
MARTY RYAN**

7. PERFORMING ORGANIZATION NAME(S) AND ADDRESS(ES)

* Air Vehicle Department; Materials Division (Code 4.3.4.2)
NAVAL AIR WARFARE CENTER
AIRCRAFT DIVISION WARMINSTER
P.O. Box 5152, Warminster, PA 18974-0591

8. PERFORMING ORGANIZATION REPORT NUMBER

NAWCADWAR-95027-4.3

9. SPONSORING / MONITORING AGENCY NAME(S) AND ADDRESS(ES)

Dr. Asha Varma
Group Head Engineering (Code 4.0C)
NAVAL AIR WARFARE CENTER; AIRCRAFT DIVISION WARMINSTER
P.O. Box 5152
Warminster, PA 18974-0591

10. SPONSORING / MONITORING AGENCY REPORT NUMBER

11. SUPPLEMENTARY NOTES

**NAVMAR APPLIED RESEARCH CORPORATION
Warminster, PA 18974

12a. DISTRIBUTION / AVAILABILITY STATEMENT

Approved for Public Release; Distribution is Unlimited.

12b. DISTRIBUTION CODE

13. ABSTRACT *(Maximum 200 words)*

Photoinduced Bragg Grating in optical fibers were first demonstrated by Hill et al. in 1978. In 1988 Meltz, et al. developed an external Bragg grating writing technique which had more flexibility in the choice of the Bragg period. Since then and due to their unique properties a number of sensing concepts have been proposed and demonstrated. Most of these sensors are configured as back reflectors. A more general configuration, a Tapped Bragg Grating (TBG), was first demonstrated by Meltz et al. in 1991. A complete theory for the fabrication and operation of TBG's is still incomplete.

In this report a simple model of Tapped Bragg Gratings is developed. This model will allow the understanding of the basic parameters necessary to fabricate TBG's. Several questions have to be answered to effectively fabricate a TBG sensor. Some of these questions are: What must the Bragg angle and period (θ_B and Δ_B) be in order to effectively scatter radiation out of the fiber at a desired scattering angle θ? How is the energy spread out of the fiber for a given θ_B and Δ_B? and What is the band pass of the scattered radiation for a given θ_B and Δ_B (this information is important to determine how many sensors can be placed in a single fiber)?

In section II the model and the TBG fabrication parameters will be described. This is the largest section and will be subdivided into several smaller sections. These subsections include "The Induced Current Approximation," "Induced Current Expansion," "Vector Potential Calculation." The band pass of a Bragg grating and the band pass of a TBG will be calculated for two different fiber modes in section III. Section IV will calculate the Poynting Vector and Scattered Power. Section V will show how the energy is spread out of the fiber for two different fiber modes. Finally in section VI the summary and conclusions will be given.

14. SUBJECT TERMS

PHOTOINDUCED BRAGG GRATING,
FIBER INDUCED BRAGG GRATING MODEL

15. NUMBER OF PAGES

16. PRICE CODE

17. SECURITY CLASSIFICATION OF REPORT	18. SECURITY CLASSIFICATION OF THIS PAGE	19. SECURITY CLASSIFICATION OF ABSTRACT	20. LIMITATION OF ABSTRACT
UNCLASSIFIED	UNCLASSIFIED	UNCLASSIFIED	SAR

FIBER OPTIC BRAGG GRATING MODEL

Ignacio Perez, Thomas Bibby
Naval Air Warfare Center
Aircraft Division
Warminster, PA 18974

Marty Ryan
Navmar Applied Research Corporation
Warminster, PA 18974

I. INTRODUCTION

Photoinduced Bragg Grating in optical fibers were first demonstrated by Hill et al.[1] in 1978. In 1988 Meltz, et al.[2] developed an external Bragg grating writing technique which had more flexibility in the choice of the Bragg period. Since then and due to their unique properties a number of sensing concepts have been proposed and demonstrated.[3,4] Most of these sensors are configured as back reflectors. A more general configuration, a Tapped Bragg Grating (TBG) (see Fig. 1), was first demonstrated by Meltz et al.[5] in 1991. A complete theory for the fabrication and operation of TBG's is still incomplete.

In this paper a simple model of Tapped Bragg Gratings is developed. This model will allow the understanding of the basic parameters necessary to fabricate TBG's. Several questions have to be answered to effectively fabricate a TBG sensor. Some of these questions are: What must the Bragg angle and period (θ_B and Λ_B) be in order to effectively scatter radiation out of the fiber at a desired scattering angle θ (refer to Fig. 1 for a graphical definition of the parameters)?, How is the energy spread out of the fiber for a given θ_B and Λ_B? and what is the band pass of the scattered radiation for a given θ_B and Λ_B? (this information is important to determine how many sensors can be placed in a single fiber).

In section II the model and the TBG fabrication parameters will be described. This is the largest section and will be subdivided into several smaller sections. This subsections include "The Induced Current Approximation", "Induced Current Expansion", "Vector Potential Calculation". The band pass of a Bragg grating and the band pass of a TBG will be calculated for two different fiber modes in section III. Section IV will calculate the Poynting Vector and Scattered Power. Section V will show how the energy is spread out of the fiber for two different fiber modes. Finally in section VI the summary and conclusions will be given.

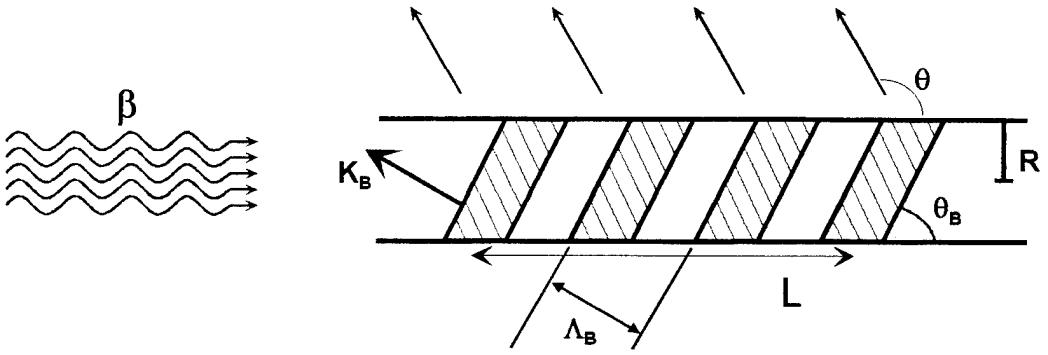

Fig.1. Basic parameters used in the model

II. TBG MODEL

To answer the questions addressed in the introduction, the induced current approximation[6] will be used to model the effects of a TBG in an optical fiber. This section will be devided into three subsections. Section IIa will introduce the induced current approximation. Section IIb will expand the current into its cartesian coordinates. Section IIc will calculate the vector potential from where the scattering fields will be determined.

IIa. The Induced Current Approximation

In the induced current approximation, radiation fields produced by perturbations to the index of refraction of the core of optical fibers are assumed to originate from induced currents in the fiber. These currents take the form of[6]

$$J = i\left(\frac{\varepsilon_O}{\mu_O}\right)^{1/2} k\cdot(n_0^2 - n^2)\cdot E \tag{1}$$

where n_o^2-n^2 is the square of the differences of the perturbed to unperturbed index of refraction, E is the unperturbed electric field inside the core of the fiber, and k is the wave number. Assuming that the fiber axis is along the z-direction and that K_B is in the x-z plane, then the quantity n_o^2-n^2 in Eq. 1 can be modeled by a simple trigonometric function

$$\begin{aligned} n_0^2 - n^2 &= 2n_0\Delta n\cdot\cos(\vec{K}_B\cdot\vec{r}') \\ &= 2n_o\Delta n\cdot\ \theta(R-r)\cdot\theta(L/2-|z|)\cos\{x\,K_B\cos(\theta_B)\ -\ z\,K_B\sin(\theta_B)\} \end{aligned} \tag{2}$$

where Δn is the difference in the index of refraction of the perturbed to unperturbed regions in the fiber core. The step functions in Eq. 2 are used to define the extent of the TBG. The argument of the cosine is the dot product of the Bragg wave number (K_B=2π/Λ_B) times the position vector in Cartesian coordinates. Figure 1 shows a graphical representation of the parameters used in this model. The electric field in Eq. 1 will depend on the mode traveling in the fiber. There are two modes that will be

considered in this paper, hybrid modes and transverse modes. For a hybrid field mode the electric is given by[7]

$$E(r,\phi,z) = \vec{e}(r,\phi)\cdot e^{i\beta z}$$

$$\vec{e} = e_r(r,\phi)\cdot\hat{e}_r + e_\phi(r,\phi)\cdot\hat{e}_\phi + e_z(r,\phi)\cdot\hat{e}_z$$

$$e_r(r,\phi) = -\frac{a_1 J_{\nu-1}(u\frac{r}{R}) + a_2 J_{\nu+1}(u\frac{r}{R})}{J_\nu(u)} f_\nu(\phi)$$

$$e_\phi(r,\phi) = -\frac{a_1 J_{\nu-1}(u\frac{r}{R}) - a_2 J_{\nu+1}(u\frac{r}{R})}{J_\nu(u)} g_\nu(\phi) \qquad (3)$$

$$e_z(r,\phi) = -\frac{iu}{R\beta}\frac{J_\nu(u\frac{r}{R})}{J_\nu(u)} f_\nu(\phi)$$

where

$$f_\nu(\phi) = \begin{cases}\cos(\nu\phi), & \text{for even } \nu \\ \sin(\nu\phi), & \text{for odd } \nu\end{cases} \qquad a_1 = \frac{F-1}{2}$$

and (4)

$$g_\nu(\phi) = \begin{cases}-\sin(\nu\phi), & \text{for even } \nu \\ \cos(\nu\phi), & \text{for odd } \nu\end{cases} \qquad a_2 = \frac{F+1}{2}$$

$$F = \left(\frac{v}{uw}\right)^2 \frac{\nu}{b_1 + b_2};\quad b_1 = \frac{1}{2u}\left\{\frac{J_{\nu-1}(u)}{J_\nu(u)} - \frac{J_{\nu+1}(u)}{J_\nu(u)}\right\};\quad b_2 = \frac{1}{2w}\left\{\frac{K_{\nu-1}(w)}{K_\nu(w)} + \frac{K_{\nu+1}(w)}{K_\nu(w)}\right\} \qquad (5)$$

$$u = R(k^2 n_{co}^2 - \beta^2)^{1/2}\ ;\ w = R(\beta^2 - k^2 n_{cl}^2)^{1/2}\ ;\ v = Rk(n_{co}^2 - n_{cl}^2)^{1/2}$$

For a transverse field mode the electric field has only one component and is given by

$$E = -\frac{J_1(u\frac{r}{R})}{J_1(u)}\cdot e^{i\beta z}\cdot e_\phi \qquad (6)$$

The induced current approximation, therefore, assumes that a Bragg grating is formed by a large coherent collection ($N = L/\Lambda_B$) of identical radiators and does not take into account multiple scattering effects between them. The first approximation (identical radiators) breaks down for long gratings since the intensity of the electric field will drop as energy is scattered out of the fiber. The second approximation (no multiple scattering effects) breaks down as the Bragg angle approaches 180° (the so-called back reflection mode). In the limit of small reflection coefficient for each Bragg line (which is the case

for most fiber Bragg gratings) only the first reflection will be significant and the second approxdimation will remain valid .

IIb. Induced Current Expansion

All of the calculations in this effort will be performed in a Cartesian coordinates system. Therefore, by transforming the induced current (Eq. 1) into this coordinate system it is simple to show that

$$\begin{aligned} J_x &= a \cdot E_x = a \cdot e_r \cos(\phi) - a \cdot e_\phi \sin(\phi) \\ J_y &= a \cdot E_x = a \cdot e_r \sin(\phi) + a \cdot e_\phi \cos(\phi) \\ J_z &= a \cdot e_z \end{aligned} \tag{7}$$

where, for clarity, all the parameters (except for the electric field components) have been absorbed in the parameter "a". By separating the "even" and "odd" terms, it can be easily shown that for the hybrid modes

$$\begin{aligned} J_x^{even} &= -a\left[a_1 \frac{J_{\nu-1}(u\frac{r}{R})}{J_\nu(u)} \cos(1-\nu)\phi + a_2 \frac{J_{\nu+1}(u\frac{r}{R})}{J_\nu(u)} \cos(1+\nu)\phi \right] \cdot e^{i\beta z} \\ J_x^{odd} &= -a\left[-a_1 \frac{J_{\nu-1}(u\frac{r}{R})}{J_\nu(u)} \sin(1-\nu)\phi + a_2 \frac{J_{\nu+1}(u\frac{r}{R})}{J_\nu(u)} \sin(1+\nu)\phi \right] \cdot e^{i\beta z} \\ J_y^{even} &= -a\left[a_1 \frac{J_{\nu-1}(u\frac{r}{R})}{J_\nu(u)} \sin(1-\nu)\phi + a_2 \frac{J_{\nu+1}(u\frac{r}{R})}{J_\nu(u)} \sin(1+\nu)\phi \right] \cdot e^{i\beta z} \\ J_y^{odd} &= -a\left[a_1 \frac{J_{\nu-1}(u\frac{r}{R})}{J_\nu(u)} \cos(1-\nu)\phi - a_2 \frac{J_{\nu+1}(u\frac{r}{R})}{J_\nu(u)} \cos(1+\nu)\phi \right] \cdot e^{i\beta z} \end{aligned} \tag{8}$$

$$J_z = -\frac{iu}{R\beta} \frac{J_\nu(u\frac{r}{R})}{J_\nu(u)} \begin{Bmatrix} \cos(\nu\phi) \\ \sin(\nu\phi) \end{Bmatrix} \cdot e^{i\beta x} \quad \begin{matrix} \text{even} \\ \text{odd} \end{matrix} \tag{9}$$

and for the transverse modes

$$J_x = -a \cdot \frac{J_1(u\frac{r}{R})}{J_1(u)} \sin\phi \cdot e^{i\beta z}$$

$$J_y = +a \cdot \frac{J_1(u\frac{r}{R})}{J_1(u)} \cos\phi \cdot e^{i\beta z} \qquad (10)$$

$$J_z = 0$$

IIc. Vector Potential Calculation

From the analytical expressions of the induced currents (Eqs. 8 - 10), the radiation fields can be calculated using standard antenna theory, that is, by calculating the vector potential

$$A = \frac{\mu_o}{4\pi s} \cdot e^{ikn_{cl}s} \cdot \int_{V'} J(r',\phi',z') \cdot e^{-1ks'\cos(\chi')} \cdot dV' = \frac{\mu_o}{4\pi s} \cdot e^{ikn_{cl}s} \cdot M \qquad (11)$$

where s indicates the scattering direction and

$$s' \cdot \cos(\chi') = r' \sin(\theta) \cdot \cos(\phi - \phi') + z' \cdot \cos(\theta) \qquad (12)$$

where the primed coordinates refer to a "cylindrical" coordinate system describing the fields inside the core of the fiber, while the unprimed coordinates refer to a "spherical" coordinate system describing the scattered fields outside the fiber. Fig. 2 shows the relationship between all coordinates.

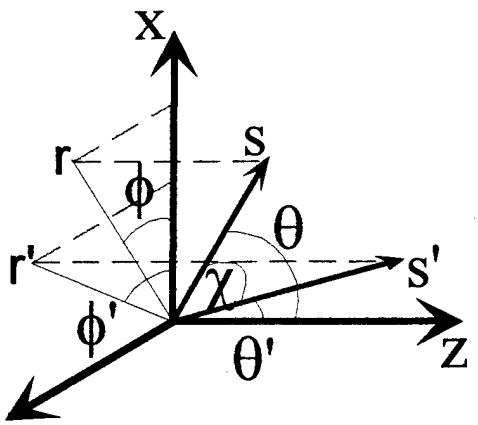

Fig. 2: Coordinate system used. s indicates the scattering direction while s' indicates a position inside the fiber.

To calculate the vector potential A, the integral in Eq. 11 will be calculated sequentially by first integrating over the variable z', then by integrating over the variable ϕ' and finally by integrating over r'.

Integral over the variable z'

The only terms containing the variable z' are in the index of refraction (Eq. **2**) and in the exponential factor exp(iβz'). These terms are common to all the components of the vector J, therefore the intagral that must be solved is

$$I_1 = \int_{-L/2}^{L/2} \cos(r' \cdot \cos(\phi') \cdot K_B \cdot \cos(\theta_B) - z' \cdot K_B \cdot \sin(\theta_B)) \cdot e^{i\beta z'} \cdot e^{-ikn_{cl}\cos(\theta) z'} dz' \qquad (13)$$

By expanding the first cosine in terms of exponentials and by introducing a new set of dummy parameters a, b, and d given by r'cos(ϕ') $K_b$cos(θ') $\rightarrow$a , K_B sin(θ_B) $\rightarrow$ b and kn_{cl}cos(θ)$\rightarrow$d) it can be easily shown that

$$I_1 = \frac{1}{2}\int_{-\frac{L}{2}}^{\frac{L}{2}} \left[e^{ia} e^{i(-b+\beta-d)z'} + e^{-ia} e^{i(b+\beta-d)z'} \right] \cdot dz' = e^{ia} \frac{\sin\left((-b+\beta-d)\cdot\frac{L}{2}\right)}{2i(-b+\beta-d)} + e^{-ia} \frac{\sin\left((b+\beta-d)\cdot\frac{L}{2}\right)}{2i(b+\beta-d)}$$

$$= e^{ir'K_B\cos(\theta_B)\cos(\phi')} \frac{\sin\left((-K_B\sin(\theta_B)+\beta-kn_{cl}\cos(\theta))\cdot\frac{L}{2}\right)}{-K_B\sin(\theta_B)+\beta-kn_{cl}\cos(\theta)} +$$

$$+ e^{-ir'K_B\cos(\theta_B)\cos(\phi')} \frac{\sin\left((K_B\sin(\theta_B)+\beta-kn_{cl}\cos(\theta))\cdot\frac{L}{2}\right)}{K_B\sin(\theta_B)+\beta-kn_{cl}\cos(\theta)}$$

Since the bound modes are always such that

$$k \cdot n_{cl} < \beta \leq k \cdot n_{co} \qquad (14)$$

only the first term will give an appreciable contribution. Therefore, I_1 reduces to

$$I_1 = e^{ir'K_B\cos(\theta_B)\cos(\phi')} \frac{\sin\left((-K_B\sin(\theta_B)+\beta-kn_{cl}\cos(\theta))\cdot\frac{L}{2}\right)}{-K_B\sin(\theta_B)+\beta-kn_{cl}\cos(\theta)} \qquad (15)$$

If the length L of the TBG is large, then I_1 will be appreciably different from zero only when the argument of the sine vanishes. From this one obtains the Bragg condition.

$$\boxed{\beta - kn_{cl}\cos(\theta_{scatt}) = K_B \sin(\theta_B)} \quad \text{First Bragg Condition} \qquad (16)$$

This is one of two equations needed to properly fabricate a TBG. It can be easily shown that this condition is simply a statement of momentum conservation along the z-direction.

Integral over the variable ϕ'

Now we will calculate the second integral, i.e., we will integrate on the azimuthal variable ϕ'. Since each component of the vector J has a different dependence on ϕ', all components will have to be calculated separately. We will first calculate the x component for the even hybrid modes. The other components and modes can be calculated similarly.

$$A_x^{even} = \frac{\mu_o}{4\pi s}\cdot e^{ikn_{cl}s}\cdot M_x^{even} \quad \text{we will only integrate } M_x^{even} \text{ on the variable } \phi'$$

$$M_x^{even} = a_1 \frac{J_{1-\nu}(u\frac{r}{R})}{J_\nu(u)}\int e^{ir'K_B\cos\theta_B\cos\phi' - ikn_{cl}r'\sin\theta\cos(\phi-\phi')}\cdot\cos(1-\nu)\phi'\cdot d\phi' \; + \; a_2 \text{ term}$$

$$= \frac{1}{2}\int e^{i(a\cdot\cos\phi' - b\cdot\cos(\phi-\phi')\pm(1-\nu)\phi'}\cdot d\phi' \quad \text{where} \quad r'K_B\cos\theta_B \to a \quad \text{and} \quad kn_{cl}r'\sin\theta \to b$$

$$= \frac{1}{2}\int e^{iQ\cos(\psi-\phi')\pm(1-\nu)\phi'}\cdot d\phi' \quad \text{where Q and } \chi \text{ are defined below}$$

$$= -\frac{1}{2}\int e^{iQ\cos\chi'\mp(1-\nu)(\psi-\chi')}\cdot d\chi' \quad \text{where we have made the replacement} \quad \psi - \phi' \to \chi'$$

$$= -\frac{e^{\pm i(1-\nu)\psi}}{2}\int e^{iQ\cos\chi'\mp(1-\nu)\chi'}\cdot d\chi' \quad \text{if we use the identity} \quad J_n(x) = \frac{i^{-n}}{2\pi}\int e^{i\cdot(x\cdot\cos(\theta)+n\cdot\theta)}\cdot d\theta$$

$$= -\frac{e^{\pm i(1-\nu)\psi}}{2}\cdot\frac{2\pi}{i^{\pm(1-\nu)}}J_{\mp(1-\nu)}(Q)$$

$$M_x^{even} = 2\pi\cdot i^{\nu-1}\left[-a_1\frac{J_{\nu-1}(u\frac{r}{R})}{J_\nu(u)}\cdot J_{\nu-1}(Q)\cos(\nu-1)\psi + a_2\frac{J_{\nu+1}(u\frac{r}{R})}{J_\nu(u)}\cdot J_{\nu+1}(Q)\cos(\nu+1)\psi\right] \qquad (17)$$

where

$$Q^2 = a^2 + b^2 - 2ab\cos(\phi)$$
$$tg(\psi) = \frac{-b\sin(\phi)}{a - b\cos(\phi)} \qquad (18)$$

and

$$a = r' K_B \cos(\theta_B)$$
$$b = r' k n_{cl} \sin(\theta) \tag{19}$$

in a similar way, it can be shown that for the other components

$$M_x^{odd} = 2\pi \cdot i^{\nu-1}\left[a_1 \frac{J_{\nu-1}(u\frac{r}{R})}{J_\nu(u)} \cdot J_{\nu-1}(Q)\sin(\nu-1)\psi + a_2 \frac{J_{\nu+1}(u\frac{r}{R})}{J_\nu(u)} \cdot J_{\nu+1}(Q)\sin(\nu+1)\psi \right]$$

$$M_y^{even} = 2\pi \cdot i^{\nu-1}\left[a_1 \frac{J_{\nu-1}(u\frac{r}{R})}{J_\nu(u)} \cdot J_{\nu-1}(Q)\sin(\nu-1)\psi - a_2 \frac{J_{\nu+1}(u\frac{r}{R})}{J_\nu(u)} \cdot J_{\nu+1}(Q)\sin(\nu+1)\psi \right]$$

$$M_y^{odd} = 2\pi \cdot i^{\nu-1}\left[a_1 \frac{J_{\nu-1}(u\frac{r}{R})}{J_\nu(u)} \cdot J_{\nu-1}(Q)\cos(\nu-1)\psi + a_2 \frac{J_{\nu+1}(u\frac{r}{R})}{J_\nu(u)} \cdot J_{\nu+1}(Q)\cos(\nu+1)\psi \right]$$

$$M_z = -2\pi \frac{iu}{R\beta} \frac{J_\nu(u\frac{r}{R})}{J_\nu(u)} \cdot \begin{cases} -i^\nu J_\nu(Q)\cdot\cos(\nu\psi) & \nu = \text{even} \\ i^\nu J_\nu(Q)\cdot\sin(\nu\psi) & \nu = \text{odd} \end{cases} \tag{20}$$

For the transverse modes it can be shown following the same procedure as for the hybrid modes that

$$M_x = +2\pi i \frac{J_1(u\frac{r}{R})}{J_1(u)} \cdot J_1(Q)\sin(\psi)$$
$$M_y = -2\pi i \frac{J_1(u\frac{r}{R})}{J_1(u)} \cdot J_1(Q)\cos(\psi) \tag{21}$$
$$M_z = 0$$

where the values of $Q = r \cdot q$ and ψ are the same as defined before

$$Q = (a^2 + b^2 - 2ab\cos(\phi))^{1/2} = r' \cdot q \quad \text{and} \quad tg(\psi) = -\frac{k n_{cl} \sin(\theta)\sin(\phi)}{K_B \cos(\theta_B) - k n_{cl} \sin(\theta)\cos(\phi)}$$

where

$$q = (K_B^2 \cos^2(\theta_B) + k^2 n_{cl}^2 \sin^2(\theta) - 2kn_{cl}K_B \sin(\theta)\cos(\theta_B)\cos(\phi))^{1/2} \quad (22)$$

The behavior of the angle ψ as a function of θ and ϕ can be seen in Fig. 3.

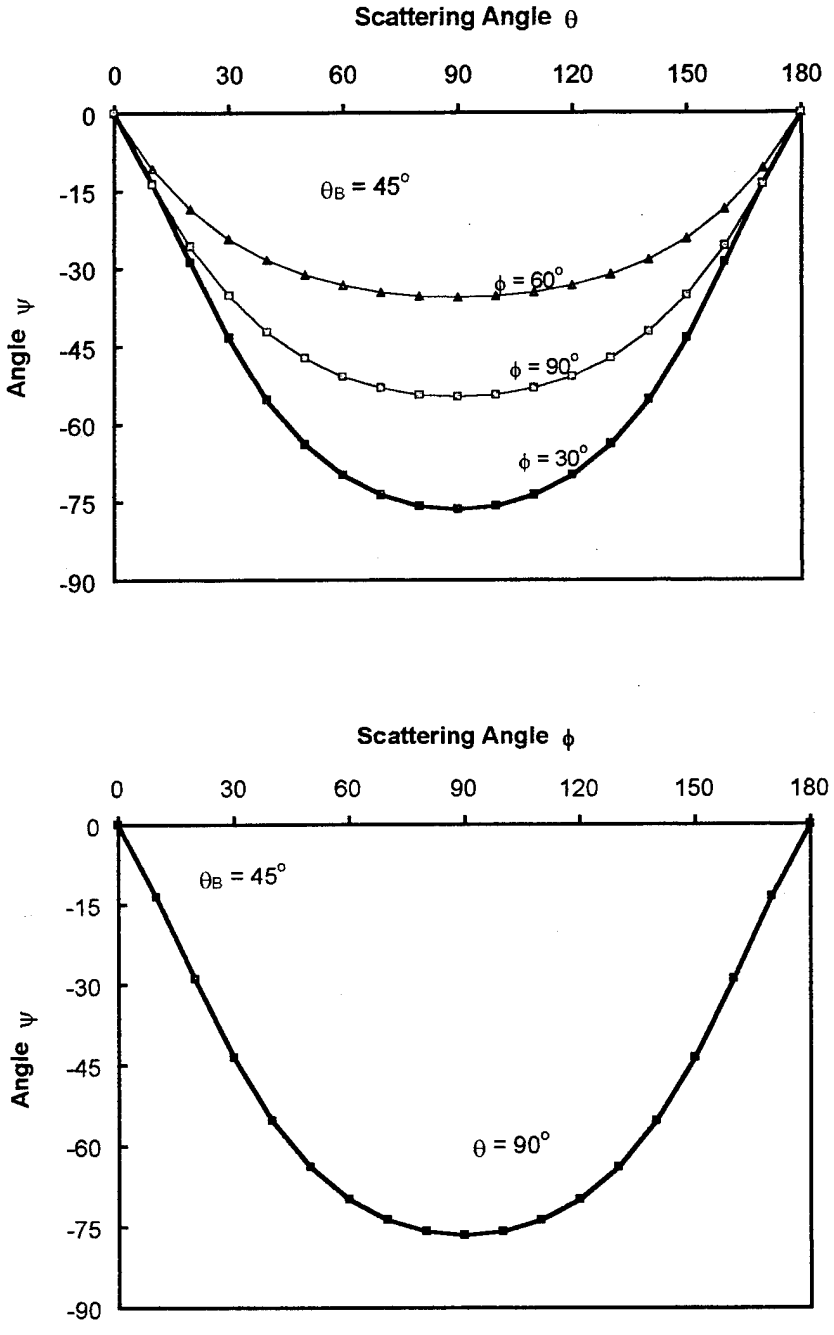

Fig. 3: variation of the angle Ψ as a function of the scatering angles θ (top) and ϕ (bottom)

Integral over the variable r'

Now we will calculate the third integral, i.e., we will integrate M over the variable r'. Since each component of the vector M has a different dependence on r', each component must be calculated separately. All of the integrals are of a similar type and the following relations will be useful

$$\int_0^R r \cdot J_m(a \cdot r) \cdot J_m(b \cdot r) \cdot dr = \frac{R}{a^2 - b^2}\left\{b \cdot J_m(a \cdot R) \cdot J_{m-1}(b \cdot R) - a \cdot J_m(b \cdot R) \cdot J_{m-1}(a \cdot R)\right\} \tag{23}$$

and

$$J_{-m}(x) = (-1)^m J_m(x) \tag{24}$$

then, it is obtained for the hybrid modes

$$M_x^{even} = 2\pi \cdot i^{\nu-1}\left[-\frac{a_1 \cdot R \cdot \cos(\nu-1)\psi}{\left(\frac{u}{R}\right)^2 - q^2}\left\{q \cdot J_{\nu-1}(u)\frac{J_{\nu-2}(qR)}{J_\nu(u)} - \frac{u}{R} \cdot J_{\nu-1}(qR)\frac{J_{\nu-2}(u)}{J_\nu(u)}\right\} + \right. \tag{25}$$

$$\left. + \frac{a_2 \cdot R \cdot \cos(\nu+1)\psi}{\left(\frac{u}{R}\right)^2 - q^2}\left\{q \cdot J_{\nu+1}(u)\frac{J_\nu(qR)}{J_\nu(u)} - \frac{u}{R} \cdot J_{\nu+1}(qR)\right\}\right]$$

$$M_x^{odd} = 2\pi i^{\nu-1}\left[-\frac{a_1 \cdot R \cdot \sin(\nu-1)\psi}{\left(\frac{u}{R}\right)^2 - q^2}\left\{q \cdot J_{\nu-1}(u)\frac{J_{\nu-2}(qR)}{J_\nu(u)} - \frac{u}{R} \cdot J_{\nu-1}(qR)\frac{J_{\nu-2}(u)}{J_\nu(u)}\right\} + \right. \tag{26}$$

$$\left. + \frac{a_2 \cdot R \cdot \sin(\nu+1)\psi}{\left(\frac{u}{R}\right)^2 - q^2}\left\{q \cdot J_{\nu+1}(u)\frac{J_\nu(qR)}{J_\nu(u)} - \frac{u}{R} \cdot J_{\nu+1}(qR)\right\}\right]$$

$$M_y^{even} = 2\pi \cdot i^{\nu-1}\left[\frac{a_1 \cdot R \cdot \sin(\nu-1)\psi}{\left(\frac{u}{R}\right)^2 - q^2}\left\{q \cdot J_{\nu-1}(u)\frac{J_{\nu-2}(qR)}{J_\nu(u)} - \frac{u}{R} \cdot J_{\nu-1}(qR)\frac{J_{\nu-2}(u)}{J_\nu(u)}\right\} + \right.$$

$$\left. \frac{a_2 \cdot R \cdot \sin(\nu+1)\psi}{\left(\frac{u}{R}\right)^2 - q^2}\left\{q \cdot J_{\nu+1}(u)\frac{J_\nu(qR)}{J_\nu(u)} - \frac{u}{R} \cdot J_{\nu+1}(qR)\right\}\right] \tag{27}$$

$$M_y^{odd} = 2\pi \cdot i^{\nu-1}\left[\frac{a_1 \cdot R \cdot \cos(\nu-1)\psi}{\left(\frac{u}{R}\right)^2 - q^2}\left\{q \cdot J_{\nu-1}(u)\frac{J_{\nu-2}(qR)}{J_\nu(u)} - \frac{u}{R} \cdot J_{\nu-1}(qR)\frac{J_{\nu-2}(u)}{J_\nu(u)}\right\} + \right.$$

$$\left. + \frac{a_2 \cdot R \cdot \cos(\nu+1)\psi}{\left(\frac{u}{R}\right)^2 - q^2}\left\{q \cdot J_{\nu+1}(u)\frac{J_\nu(qR)}{J_\nu(u)} - \frac{u}{R} \cdot J_{\nu+1}(qR)\right\}\right] \tag{28}$$

$$M_z = 2\pi \frac{u/\beta}{\left(\frac{u}{R}\right)^2 - q^2}\left\{q \cdot J_{\nu-1}(qR) - \frac{u}{R}J_\nu(qR)\frac{J_{\nu-1}(u)}{J_\nu(u)}\right\}\begin{cases} -i^{\nu-1}\cos(\nu\theta) & \nu = \text{even} \\ i^{\nu-1}\sin(\nu\theta) & \nu = \text{odd} \end{cases} \tag{29}$$

and in a similar way for the transverse modes

$$M_x = +2\pi i \frac{R\sin(\psi)}{\left(\frac{u}{R}\right)^2 - q^2}\left\{q \cdot J_0(qR) - \frac{u}{R}J_1(qR)\frac{J_0(u)}{J_1(u)}\right\}$$

$$M_y = -2\pi i \frac{R\cos(\psi)}{\left(\frac{u}{R}\right)^2 - q^2}\left\{q \cdot J_0(qR) - \frac{u}{R}J_1(qR)\frac{J_0(u)}{J_1(u)}\right\} \tag{30}$$

$$M_z = 0$$

From the previous equations, it can be seen that every component of the Vector Potential A has a probable singularity when $q(\theta,\phi=0)=u(\beta)/R$. For the hybrid mode case

ν=1 the previous condition gives the maximum amount of scatter. For other modes this condition gives the minimum amount of scatter. Therefore, for the $\nu = 1$ hybrid mode or for single mode fibers, $q(\theta,\phi=0)=u(\beta)/R$ gives the second Bragg condition for the fabrication of a tapped Bragg grating

$$\boxed{kn_{cl}\sin(\theta_{scatt}) = K_B\cos(\theta_B) \pm \frac{u(\beta)}{R}} \quad \text{Second Bragg Condition (31)}$$

Eqs. 16 and 31 completely specify the Bragg parameter (K_B, θ_B) when the propagation constant β and the desired scattering angle θ_{scatt} are given. It can be shown that Eq. 31 is a statement of the conservation of momentum along a direction normal to the fiber and in the plane containing the Bragg vector. The ambiguity in Eq. 31 (the $\pm$ ambiguity) can be removed by eliminating the last term or by working in the weak guidance approximation $u \rightarrow 0$. Eqs. 16 and 31 reduce to

$$\boxed{\begin{aligned} K_B &= 2kn_{cl}\sin(\theta_{scatt}/2) \\ \theta_B &= \theta_{scatt}/2 \end{aligned}} \qquad (32)$$

Equations 32 are the basic equations that must be satisfied to fabricate a Bragg grating. Fig. 4 shows what the Bragg period Λ_B should be in order to maximize the amount of scattered radiation in a particular scattering direction θ_{scatt} (θ_{scatt} is measured relative to the fiber axis direction). The Bragg angle θ_B is simply half of the scatter angle as shown in Eq. 32. This result answers the first question that was addressed in the introduction, i.e., what must the Bragg angle and period (θ_B and Λ_B) be in order to

$$\Lambda_B = \frac{\lambda}{2\cdot n_{cl}\cdot\sin(\theta/2)}$$

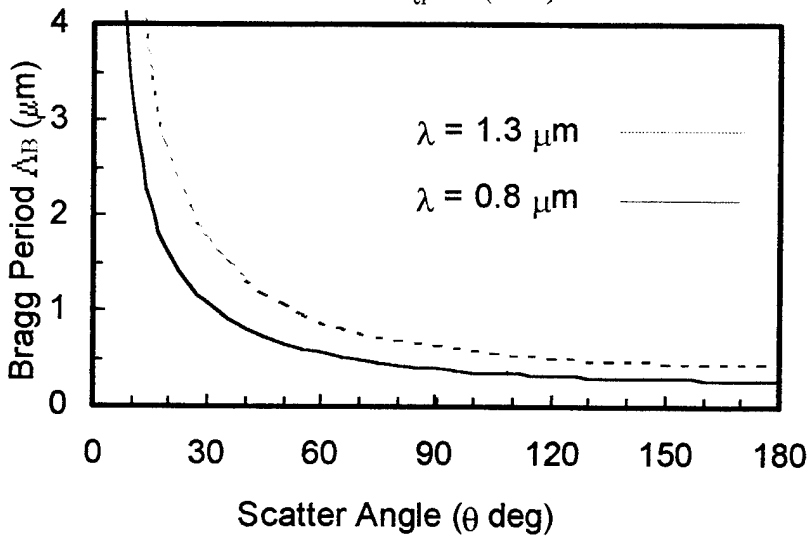

Fig. 4: Bragg period as a function scattering angle when ncl = 1.44 and for two different wavelengths

effectively scatter radiation out of the fiber at a desired scattering angle θ_{scatt}. In the weak guidance approximation ($u \to 0$), the expressions for M can be simplified by using the following relations

$$J_\nu(x \to 0) = \frac{x^\nu}{2^\nu \cdot \nu!} \; ; \quad K_{\nu-1}(x \to 0) = \frac{(\nu-1)!}{2}\left(\frac{2}{x}\right)^\nu \; ; \quad J_{\nu-1}(x) + J_{\nu+1}(x) = \frac{2\nu}{x} J_\nu(x) \tag{33}$$

in this approximation the parameters b_1, b_2, F, a_1 and a_2 converge to the following expressions

$$b_1 \to \frac{\nu}{u^2}; \quad b_2 \to -\frac{\nu}{w^2}; \quad F \to 1 + 2\frac{u^2}{v^2} \; ; \quad a_1 \to \frac{u^2}{v^2} \; ; \quad a_2 \to 1 + \frac{u^2}{v^2} \tag{34}$$

by replacing Eqs. 33 and 34 into Eqs. 25 - 28 the following approximations are obtained

$$M_x^{even} = 2\pi \cdot i^{\nu-1} \frac{\cos(\nu-1)\psi}{q^2} \cdot 2 \cdot \nu \frac{qR}{v} J_\nu(qR) \approx 2\pi R^2 \nu \cos(\nu-1)\psi \cdot \frac{J_\nu(qR)}{qR}$$

$$M_x^{odd} = 2\pi \cdot i^{\nu-1} \frac{\sin(\nu-1)\psi}{q^2} \cdot 2 \cdot \nu \frac{qR}{v} J_\nu(qR) \approx 2\pi R^2 \nu \sin(\nu-1)\psi \cdot \frac{J_\nu(qR)}{qR}$$

$$M_y^{even} = 2\pi \cdot i^{\nu-1} \frac{\sin(\nu-1)\psi}{q^2} \cdot 2 \cdot \nu \frac{qR}{v} J_\nu(qR) \approx 2\pi R^2 \nu \sin(\nu-1)\psi \cdot \frac{J_\nu(qR)}{qR} \tag{35}$$

$$M_y^{odd} = 2\pi \cdot i^{\nu-1} \frac{\cos(\nu-1)\psi}{q^2} \cdot 2 \cdot \nu \frac{qR}{v} J_\nu(qR) \approx 2\pi R^2 \nu \cos(\nu-1)\psi \cdot \frac{J_\nu(qR)}{qR}$$

$$M_z = 0$$

we have only retained the terms of the form ν^{-1}. For the transverse modes it can be easily shown that

$$\begin{aligned} M_x &= i \cdot 2\pi R^2 \cdot \sin(\psi) \frac{J_2(qR)}{qR} \\ M_y &= i \cdot 2\pi R^2 \cdot \cos(\psi) \frac{J_2(qR)}{qR} \\ M_z &= 0 \end{aligned} \tag{36}$$

III. TBG BAND PASS

For the case of back reflection ($\theta_B = 90^\circ$ and $\theta_{scatt} = 180^\circ$) it can be shown (by forcing the argument of the sine of Eq. 15 to be $\pm \pi/2$) that the spectral width of the reflected energy is given by

$$\Delta\lambda = \frac{\lambda_o}{2 \cdot N} \tag{37}$$

where λ_o is the wavelength in vacuum, and N is the number of lines in the grating defined from $L = N \cdot \Lambda_B$. Clearly as the number of lines in the Bragg grating increase, the width of the reflected component narrows. For a grating with N = 10,000 lines, the reflected width for a beam with wavelength of λ_o =1 μm would give $\Delta\lambda$ = 0.1 nm. Such a grating would only measure $L = N \cdot \Lambda_B = N \cdot \lambda_o/(2 \cdot n_{cl})$ = 3 mm (assuming that n_{cl} = 1.5).

One of the great advantages of Bragg gratings is that, due to the extreme spectral narrowness of the reflected component[8] (on the order of $\Delta\lambda$ = 0.1 nm), many Bragg gratings can be placed in a single fiber with the possibility of interrogating each grating independantly. This can be done by fabricating each grating in the fiber with a different Bragg period Λ_B and then interrogating all the gratings with a broad band signal (BBS). If the spectral width of the BBS signal is $\Delta\lambda_{BBS}$ = 50 nm, centered at λ = 1300 nm in a fiber of index n = 1.4 and the desired strains to measured are of the order of ε = 1,000 μstrains, then the number of sensors that could be independently addressed would be $Nsensor = \Delta\lambda_{BBS}/(2n\lambda\varepsilon)$ = 50/3.6 = 13 sensors. Notice that in this case the reflected spectral spread for the desired strain measurements is $\Delta\lambda_{strain} = 2n\lambda\varepsilon$ = 3.6 nm which is much larger than the spectral width of the reflected signal $\Delta\lambda$ = 0.1 nm. Therefore it is this parameter, $\Delta\lambda_{strain}$, that dictates the number of sensors that will fit in a fiber without overlap as opposed to $\Delta\lambda$. The ability of placing many sensors in a single optical fiber and of being able to interrogate each sensor independently has many potential applications, specially in the area of smart materials where the stress state of an entire panel can be monitored with a single optical fiber.

The spectral width of the scattered energy when the Bragg angle is smaller than $\theta_B = 180^\circ$ is much larger. The basic reason for this is that different wavelength can effectively scatter out of a fiber at different angles, i.e., the scattering angle is not fixed as happened in the backscattering case described above. The spectral width for this more general case will be discussed later in this section. For now we will calculate the angular spread of a monochromatic (fixed wavelength λ) beam reflected out of a fiber. This can be easily obtained by forcing the argument of Eq. 15 to be equal to $\pm \pi/2$, then

$$\Delta\theta \approx \frac{\lambda_o}{n_{cl} \cdot L \cdot \sin(\theta)} \tag{38}$$

notice that the beam can be extremely narrow as L, the length of the grating, increases. In general the limiting factor defining the angular spread of the beam is not the length L of the grating as we have just shown, but the spectral content $\Delta\lambda$ of the beam, as will be shown next.

In the case of a TBG the situation is different from above because now for a set of Bragg parameters (K_B and θ_B) there will be a broad range of propagation constants β (and therefore wavelengths) that will satisfy Eq. 16 for different scattering angles. In the weak guidance approximation ($u \rightarrow 0$ or $\beta \rightarrow kn_{cl}$) the expression for the spectral width ($\Delta\lambda$) in terms of the angular spread $\Delta\theta$ can be obtained by differentiation ($d\lambda/d\theta$) of Eq. 16

$$\Delta\lambda = \lambda \cdot \frac{\Delta\theta}{\tan\left(\frac{\theta_{scatt}}{2}\right)} \tag{39}$$

The angular spread, $\Delta\theta$, can be calculated by determining the angle at which Eq. 35 or 36 has its first zero for $\phi=0$. In the weak guidance approximation the function $A(\theta,\phi)$ can be written as

$$A(\theta,\phi) \propto \frac{J_n(q \cdot R)}{q \cdot R} \cdot \delta(K_B \cos(\theta_B) - 2kn_{cl} \sin(\theta)) \tag{40}$$

The zeros of the previous equation are the zeros of the nth order Bessel function. Therefore we get

$$\begin{aligned} q \cdot R &= a_n \\ \sin(\theta_{scatt}) - \sin(\theta_{zero}) &= \frac{a_n}{R \cdot k \cdot n_{cl}} \end{aligned} \tag{41}$$

where a_n = 2.40, 3.83, 5.14, 6.38 .... for n = 0,1,2,3, ... are the zeros of the Bessel function.

Fig. 5 shows the angular and spectral width for two different fiber modes and two different scattering angles as a function of the Rk product. From that graph it is clear that the larger the Rk product, the smaller the diffraction effects, and therefore the narrower the angular and spectral broadening. In contrast, the larger the Rk product is the more modes that the fiber will be able to sustain and therefore more intermodal coupling effects in the fiber. For single mode operation the Rk value has to be smaller than the $2.45/(n_{cl}^2 - n_{co}^2)^{1/2}$. For a typical 10 μm core fiber Rk has a value of 60. One can see from Fig. 5 bottom that the spectral width is $\Delta\lambda$ = 0.5 μm for light scattered out of the fiber at 90°. This is more then 3 orders of magnitude bigger than in the case of a back reflecting Bragg grating. The TBG band pass can be made smaller by increasing the scattering angle as shown in Fig. 5 bottom. All these considerations will have to be taken into account when fabricating TBG sensors.

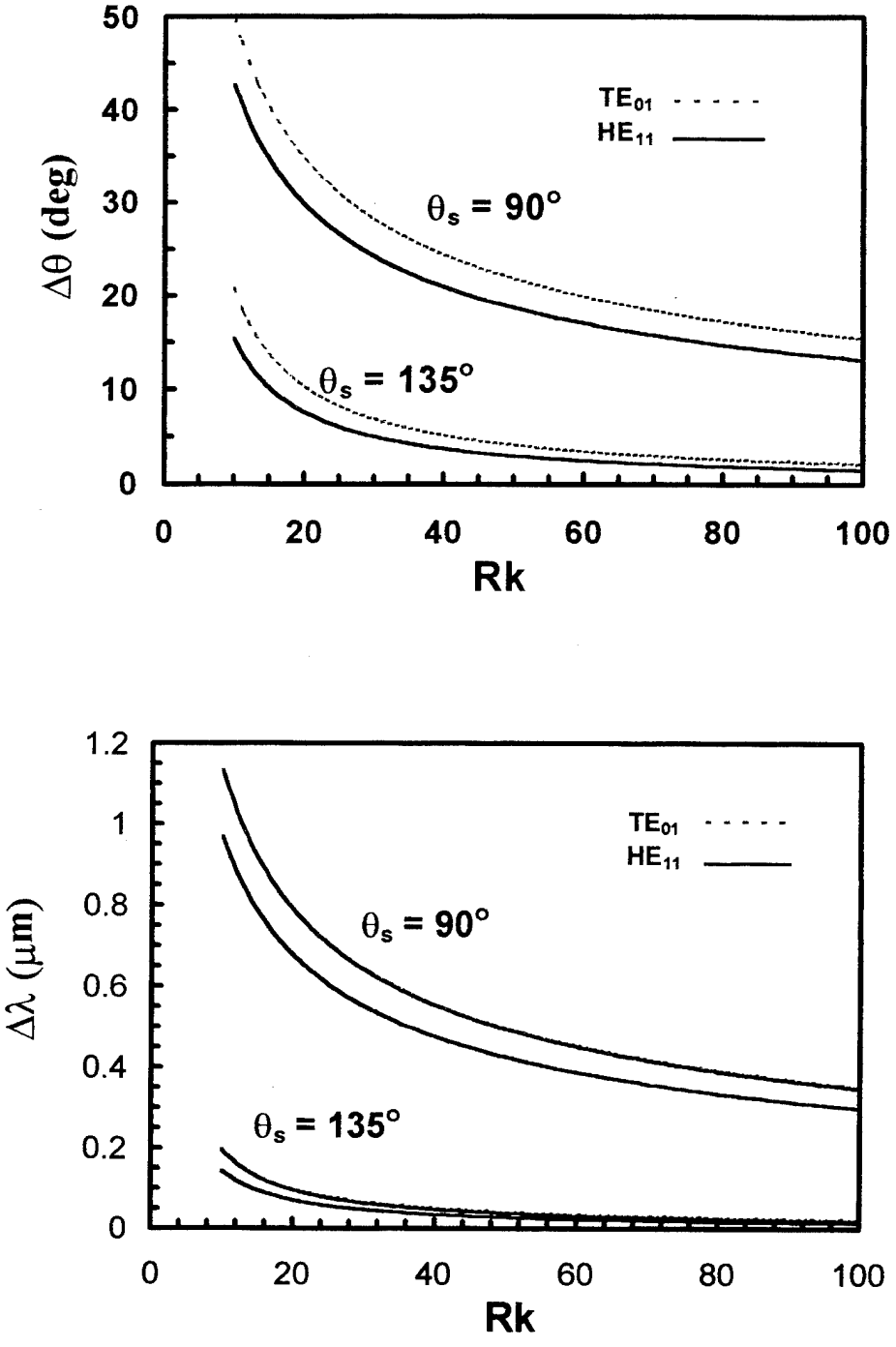

Fig. 5 Top: Angular spread of a TBG as a function of the Rk value of a fiber for two different scattering angles and two different modes. Bottom: Spectral Spread of a TBG as a function of the Rk value of a fiber for two different scattering angles and two different modes.

IV. POYNTING VECTOR CALCULATION

Finally the quantity M can be written in the weak guidance approximation as

$$M_x(\theta,\phi) = a \cdot 2\pi R^2 \nu(1+\nu)\cos(\nu-1)\psi \cdot \frac{J_\nu(qR)}{qR} \cdot \delta(-K_B \sin(\theta_B) + \beta - kn_{cl}\cos(\theta))$$

$$M_y(\theta,\phi) = a \cdot 2\pi R^2 \nu(1+\nu)\sin(\nu-1)\psi \cdot \frac{J_\nu(qR)}{qR} \cdot \delta(-K_B \sin(\theta_B) + \beta - kn_{cl}\cos(\theta)) \quad (42)$$

where "a" is a new dummy proportionality constant that contains various fiber parameters.

From the components of M one can calculate the Poynting vector S and the total radiated power

$$S = \frac{c^2 k^2 n_{cl}}{2} \cdot \left(\frac{\varepsilon_o}{\mu_o}\right)^{1/2} \cdot |r \times A|^2 \hat{r} = \frac{k^2 n_{cl}}{32\pi^2 r^2}\left(\frac{\mu_o}{\varepsilon_o}\right)^{1/2}\left\{|M_\theta|^2 + |M_\phi|^2\right\}\hat{r} \quad (43)$$

$$P_{rad} = \frac{c^2 k^2 r^2 n_{cl}}{2}\left(\frac{\varepsilon_o}{\mu_o}\right)^{1/2}\int_{S_\infty}|r \times A|^2 d\Omega = \frac{k^2 n_{cl}}{32\pi^2}\left(\frac{\mu_o}{\varepsilon_o}\right)^{1/2}\int_0^{2\pi}\int_0^{\pi}\left\{|M_\theta|^2 + |M_\phi|^2\right\}\sin(\theta)d\theta d\phi \quad (44)$$

where M_θ and M_ϕ are the components of M in a spherical coordinate system. These components can be easily calculated from the cartesian components of the vector M as shown below

$$M_\theta = M_x \cos(\theta)\cos(\phi) + M_y \cos(\theta)\sin(\phi)$$
$$M_\phi = -M_x \sin(\phi) + M_y \cos(\phi) \quad (45)$$

and since $M_x = M \sin(\nu\text{-}1)\psi$ and $M_y = M \cos(\nu\text{-}1)\psi$ as seen from Eqs. 42, then

$$M_\theta^2 + M_\phi^2 = M_x^2 + M_y^2 - \sin^2(\theta)\cdot\left(M_x\cos(\phi) + M_y\sin(\phi)\right)^2$$
$$= M^2(1 - \sin^2(\theta)\sin^2((\nu-1)\psi + \phi)) \quad (46)$$

therefore

$$S(\theta,\phi) = \frac{k^2 n_{cl}}{32\pi^2 r^2}\left(\frac{\varepsilon_o}{\mu_o}\right)^{1/2} M^2(1 - \sin^2(\theta)\sin^2((\nu-1)\psi + \phi))\cdot\hat{r} \quad (47)$$

In general, the polarization effects (which are included in the polarization factor (1 - $\sin^2(\theta)\sin^2((\nu\text{-}1)\psi+\phi)$)) are a much slowly varying function of the scattering angles θ and ϕ than the function M. As a result, Eqs. 16, 31, 32, 39 and 41 will remain valid even

though they were calculate directly from M (which is proportional to the vector potential A) rather than from the Poynting vector S which has polarization information.

The total power radiated can be calculated from

$$P_{rad} = \frac{k^2 n_{cl}}{32\pi^2}\left(\frac{\mu_o}{\varepsilon_o}\right)^{1/2} \int_o^{2\pi}\int_o^{\pi} \left\{M^2\left(1 - \sin^2(\theta)\sin^2((\nu-1)\psi + \phi)\right)\right\} \sin(\theta)\, d\theta\, d\phi \qquad (48)$$

where in the weak guidence approximation

$$M(\theta,\phi) = a \cdot 2\pi R^2 \nu(1+\nu)\frac{J_\nu(qR)}{qR} \cdot \delta(-K_B \sin(\theta_B) + \beta - k n_{cl}\cos(\theta)) \qquad (49)$$

V. ENERGY DISTRIBUTION OUT OF A TBG

The distribution of the energy out of a TBG can be calculated from Eqs. 47 and 49. From those equations it is possible to identify three parts which contain the scattering angles θ and ϕ. The first part, $[J(qR)/qR]^2$, is a rapidly varying function of the scattering angles and exhibits a singular behavior near qR=0. This contribution is the most important contribution when determining the energy distribution out of a TBG. The second part, the delta function, places a restriction to the values that the polar scatter angle θ can have (Eq. 16). This restriction can be directly incorporated into the first part. The third part is the polarization factor $(1 - \sin^2(\theta)\sin^2((\nu-1)\psi+\phi)))$ where ψ was defined in Eq. 18. Fig. 6a shows 3D image of the polarization factor while Figs. 6b and 6c show two cross sectional views in parametric format of the same polarization factor for a mode given by $\nu = 1$. It can clearly be seen from these Figures that the polarization factor is a slowly varying function of the scattering angles. Consequently, this contribution will not be important when determining the energy distribution out of a TBG.

Fig. 7a shows the first part, $[J(qR)/qR]^2$, of the energy distribution out of a TBG for two different fiber modes, the HE_{11} and the TE_{01} and for a scatter angle of $\theta_{scatt} = 90°$. Fig 7b gives a pictorial representation of how the energy is distributed inside de fiber for the same two fiber modes. Note how the node in the fiber for the TE_{01} mode translates into a butterfly shaped distribution out of the fiber. Other modes have more complicated energy distributions. The HE_{11} mode is the most effective mode for coupling energy out of an optical fiber.

Fig. 8 shows the energy distribution for different polar scatter angles ranging from $\theta = 0°$ to $\theta = 180°$ for $\phi = 0°$. Fig. 9 shows the azimuthal distribution of energy scattered out of a TBG for various scatter angles.

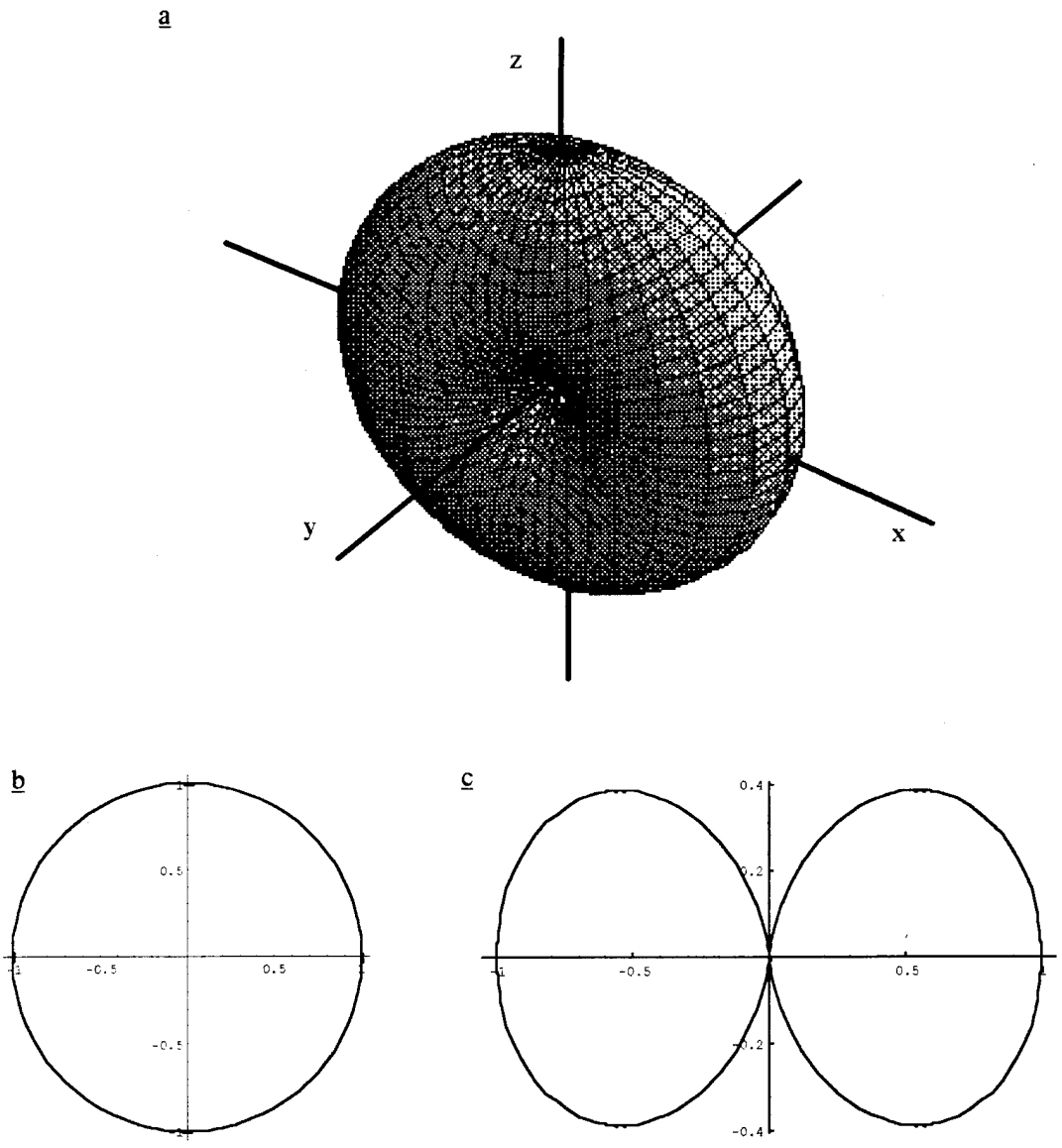

Fig. 6a. Shows a 3D parametric plot of polarization factor for the mode $\nu = 1$. 6b Shows a parametric plot of the polarization factor for $\phi = 0$, the vertical axis corresponds to the z-axis, while the horizontal axis correspondes to the x-axis. This is the polar plane. 6c. Shows a parametric plot of the polarization factor for $\theta = 90^{\circ}$, the vertical axis corresponds to the y-axis, while the horizontal axis correspondes to the x-axis. This is the azimuthal plane.

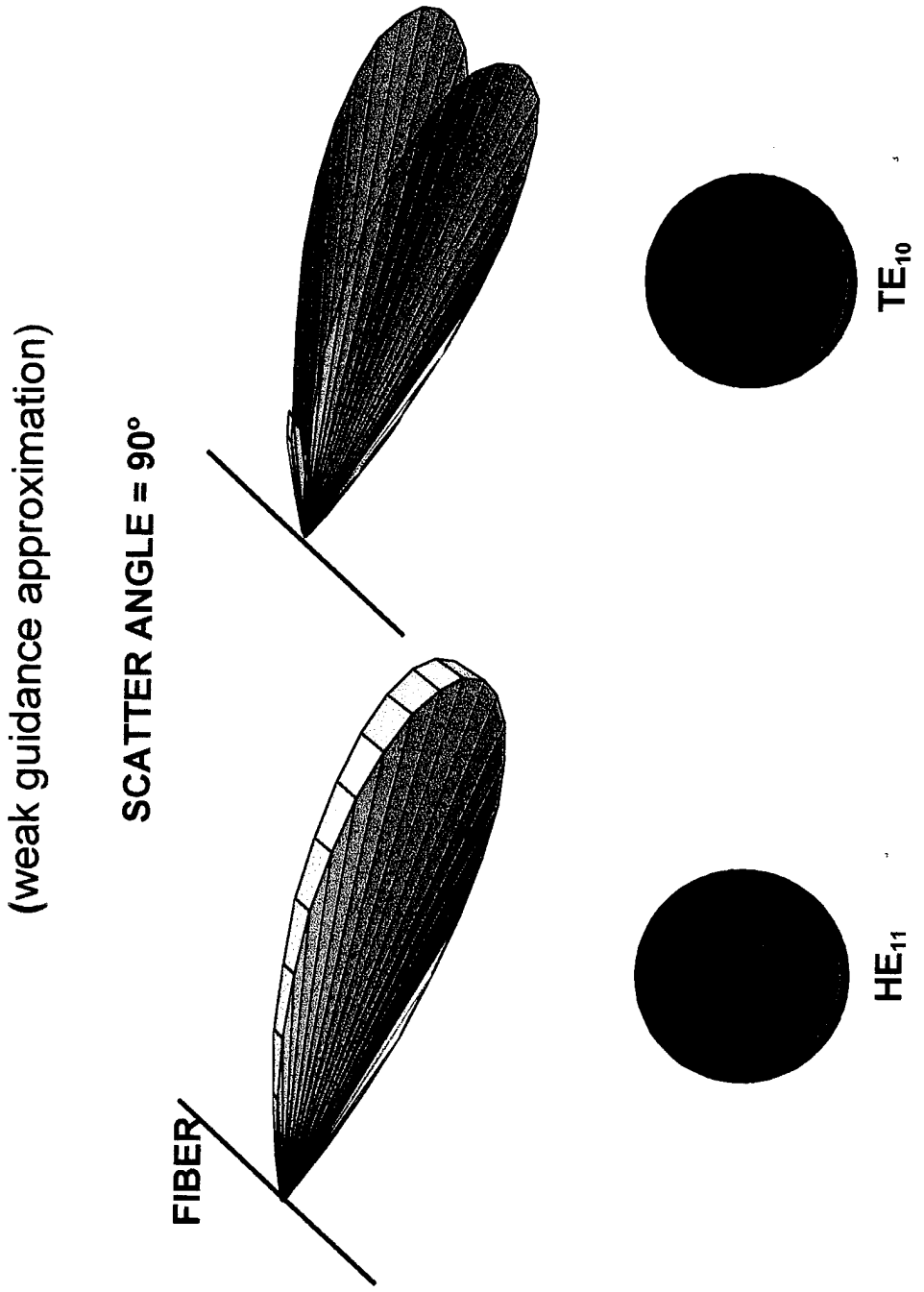

Fig. 7: shows the first part, $[J(qR)/qR]^2$, of the energy distribution out of a TBG for two different fiber modes, the HE_{11} and the TE_{01} and for a scatter angle of $\theta_{scatt} = 90^o$. Fig. 7b gives a pictorial representation of how the energy is distributed inside the fiber for the same two fiber modes as before.

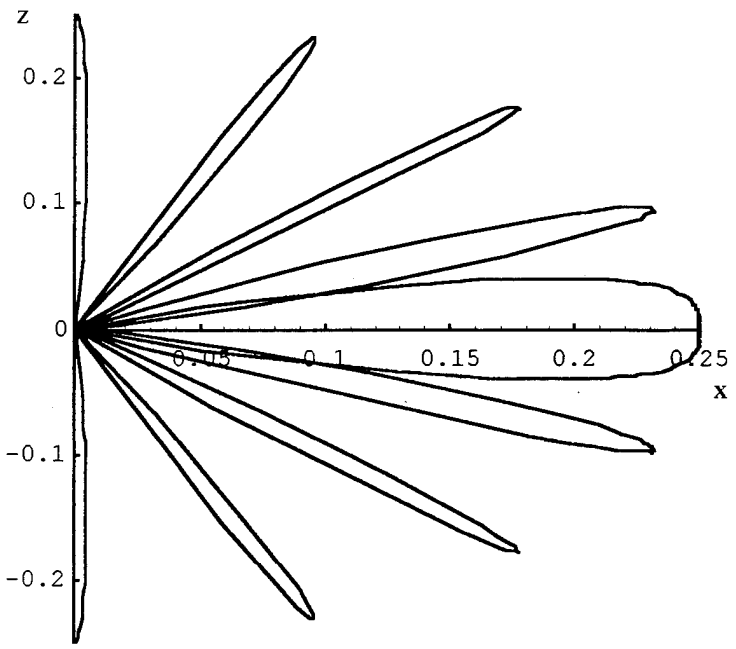

Fig. 8. Energy distribution function for various polar scatterr angles ranging from $\theta = 0^{\circ}$ to $\theta = 180^{\circ}$

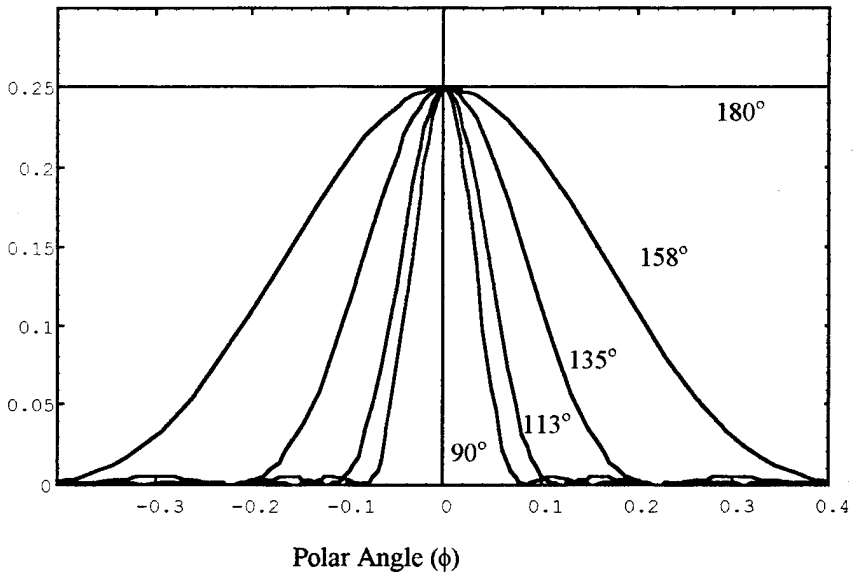

Fig. 9. Azimuthal energy distribution curves for various scattering angels.

VI. CONCLUSION

The basic model and its limitations for the fabrication of an optical fiber Tapped Bragg Grating has been amply described in section II of this work. The basic equations required to fabricate a Tapped Bragg Grating (Eqs. 16 and 31) have been derived. Eqs. 32, which are the equations normally found in the literature, are a good approximation for single mode fibers or for fiber that have a small Rk value. The angular and spectral spread of a TBG has been derived in the weak guidance approximation (Eqs. 39 and 41). From those results it was found that the spectral width of a TBG is a strongly dependent function of the scattering angle θ_{scatt} . It was also found that the spectral width of a TBG was several orders of magnitude larger than the spectral width of a standard Bragg Grating back reflector. This results significantly limits the number of TBG that can be place in a single fiber and still be able to independently interrogate them. Finally, the spatial distribution of energy out of a fiber has been derived (Eqs. 47). This result is important when using TBG for demodulation purposes or for sensor development purposes. In particular, these results are being applied for the development of a corrosion sensor in our group at the NAWCADWAR[9].

VII. ACKNOWLEDGMENT

The authors would like to thank the office of Science and Technology of the Naval Air Warfare Center at Warminster Pennsylvania for the support for this work.

1 K. O. Hill, Y. Fujii, D. C. Johnson, and B.S. Kawasaki, Appl. Phys. Lett. **32**, 647, (1978)

2 G. Meltz, W. W. Morey, and W. H. Glenn, Opt. Lett. 14, 823,(1989)

3 W.W. Morey, J.R. Dunphy, and G. Meltz, Proc. Soc. Photo-Opt. Instrum. Eng. **1586**, 216, (1991)

4 R. M. Measures, K. Liu, S. Melle, Proc. of the ADPA/AIAA/ASME/SPIE conf. on Active Materials and Adaptive Structures. (G.J. Knowles Ed) Inst. of Phys. Pub. p.301, (1991)

5 G. Meltz, W. W. Morey, and J.R. Dumphy, SPIE **1587**, 350, (1991)

6 A. W. Snyder, J. D. Love, "*Optical Waveguide Theory,*" Chapman and Hall pub., 1983, p. 460

7 A. W. Snyder, J. D. Love, "*Optical Waveguide Theory,*" Chapman and Hall pub., 1983, p. 250

8 S.M. Melle, K. Liu, R.M. Measures, *Applied Optics*, **32**, p. 3601 (1993)

9 I. Perez, V. Agarwala, W.R. Scott, S.D. Tyagi, "*Review of Progress in Quantitative Nondestructive Evaluation,*"D.O.Thompson and D.E.Chimenti eds. Plenum Press Pub., **14**, p. 2081 (1995)

DISTRIBUTION LIST

Report No. NAWCADWAR-95027-4.3

No. of Copies

Michael Kijesky 1
Naval Air Warfare Center
Aircraft Division
Code 4.5C.2
Warminster, PA 18974

James McEachern 1
Naval Air Warfare Center
Aircraft Division
Code 4.5C.1
Warminster, PA 18974

Dr. Asha Varma 1
Naval Air Warfare Center
Aircraft Division
Code 4
Warminster, PA 18974

Dr. Barry Blackley 1
Naval Underwater Warfare Center
Code 2141
New London, CT 06320

Robert Barley 3
Scientific Officer
Office of Naval Research, BCT 1
800 N. Quincy St.
Arlington, VA 22217-5660

Scott Littlefield 3
Scientific Officer
Office of Naval Research, BCT 1
800 N. Quincy St.
Arlington, VA 22217-5660

Asuri Vasudeven 1
Scientific Officer
Office of Naval Research, BCT 1
800 N. Quincy St,
Arlington, VA 22217-5660

Dr. Jeff Waldman 1
Naval Air Warfare Center
Aircraft Division
Code 4.3.4.2
Warminster, PA 18974

DISTRIBUTION LIST
Report No. NAWCADWAR-95027-4.3

No. of Copies

Dr. Lloyd Bobb 1
Naval Air Warfare Center
Aircraft Division
Code 4.5.5.2.1
Warminster, PA 18974

Dr. Warren Herman 1
Naval Air Warfare Center
Aircraft Division
Code 4.5.5.6.5
Warminster, PA 18974

Dr. Thomas J. Moran 1
Wright Laboratory
Materials Directorate
WL/MLLP Bldg. 655
Wright Patterson AFB, OH 45433-7817

Mr. Clifford W. Anderson (USNL, Act. Chm.) 1
Carderock Division
White Oak Site
Code 684
Naval Surface Warfare Center
Silver Spring, MD 20903-5640

Naval Air Warfare Center 2
Aircraft Division Warminster
Code 7.2.5.5
P.O. Box 5152
Warminster, PA 18974-0591

Defense Technical Information Center 2
ATTN: DTIC-FDAB
Cameron Station BG5
Alexandria, VA 22304-6145

Center for Naval Analysis 1
4401 Fort Avenue
P.O. Box 16268
Alexandria, VA 22302-0268